Computers and Fluids 161 (2018) 60–73

Contents lists available at ScienceDirect

Computers and Fluids

journal homepage: www.elsevier.com/locate/compfluid

Slip boundary condition for lattice Boltzmann modeling of liquid flows

Kai Wang[a], Zhenhua Chai[b], Guoxiang Hou[a,*], Wei Chen[a], Sheng Xu[c]

[a] School of Naval Architecture and Ocean Engineering, Huazhong University of Science and Technology, Wuhan, 430074, People's Republic of China
[b] School of Mathematics and Statistics, Huazhong University of Science and Technology, Wuhan, 430074, China
[c] China Ship Development and Design Center, Wuhan, 430064, China

ARTICLE INFO

Article history:
Received 26 April 2017
Revised 14 November 2017
Accepted 16 November 2017
Available online 16 November 2017

Keywords:
Slip boundary
Lattice Boltzmann
Linear slip model
Boundary condition

ABSTRACT

Boundary slip phenomenon has been widely studied for microscale gas flow in recent years. However, researches on this topic for liquid flow are still rare. Boundary slip of liquid flow is caused by roughness and micro bubbles, while that of gas flow is caused by rarefied effect. Despite this difference, researchers found that some slip boundary conditions for gas flow can also be applied to liquid flow, except the different way of treating accommodation coefficients. Currently, a measurable physical parameter, slip length, is widely used for liquid flow, which can be obtained through experiential methods. If the relationship between the slip length and the accommodation coefficients can be found theoretically, these slip boundary conditions for liquid flow will be powerful tools to research slip related flow characteristics, for example, drag reduction with superhydrophobic surface. Based on the Navier slip model, this paper deducts the relationship between the accommodation coefficients and the slip length with the halfway and the modified slip boundary conditions, under the framework of the lattice Boltzmann method (LBM). The effectiveness of the proposed slip boundary conditions are verified with the Couette flow, the Poesueille flow, the water Cu nanofluid flow, and the 2-D Womersley flow. Results indicate that these boundary conditions are suitable for both linear and non-linear liquid flow.

1. Introduction

Boundary slip phenomenon has attracted increasing attention for liquid [1–5] and gas flow [6–8] with the development of nanotechnology. The physical mechanism of boundary slip is totally different between liquid and gas flows. For micro gas flow, the Knudsen number (Kn) is small, and the continuum assumption may break down [9]. For liquid flow, the continuum assumption may be still reliable for most cases with very small Knudsen number [9]. The slip phenomenon of gas flow is caused by rarefied effect, while the slip phenomenon of liquid flow is apparent slip caused by the roughness and micro bubbles. Therefore, the Knudsen number is commonly used to characterize slip effect for gas flow, and slip length for liquid flow [10–12]. Slip length can be measured by equipments. The real slip length for liquid flow is no more than a micron, and apparent slip length of liquid flow on superhydrophobic surface can be above a hundred microns [13–15]. As important complements to experiment, numerical methods are powerful tools to study slip phenomenon. The establishment of reasonable slip boundary conditions are significant to this aim.

Among the various numerical methods, the lattice Boltzmann method (LBM) has emerged as a promising tool to simulate micro flow for its mesoscale property, great parallel capability, and simple algorithm formulation. These years, researches on slip boundary conditions based on LBM become active [16]. For flow with slip boundary, the LBM slip schemes were formulated as a previously existing rules, such as bounce back (BB), specular reflection (SR), and diffusive Maxwell's reflection model (DM). Nie et al. [17] firstly obtained a slip velocity on the solid wall with the conventional bounce back boundary condition of LBM when they were studying microchannel flows. But this slip velocity was confirmed to be a numerical artifact later [18], which attracts many attentions to solve the problem [19,20]. Meanwhile, Lim et al. [21] took the specular reflection boundary condition for slip wall. Their numerical results did not agree well with some existing analytical results, and the numerical results was sensitive to mesh size. Ansumali et al. [22] derived the diffusive Maxwells reflection boundary condition for the model of a diffusively reflecting moving solid wall. A balance parameter was added to ensure the rule of conservation of mass. To overcome the shortage of above rules, combination methods were proposed, which were the combined BB-SR method (BSR) [23–25], DM-SR method (DM) [24,26,27], and DM-BB method (DBB) [18,28]. With the ability to simulate flows with wide range of slip length, the BSR method is widely used.

* Corresponding author.
E-mail address: houguoxiang@163.com (G. Hou).

https://doi.org/10.1016/j.compfluid.2017.11.009
0045-7930/

However, slip boundary of liquid flow for LBM is still confusing. How to calculate the accommodation coefficient, r, was the main challenge of this method [29,30]. Researches on boundary slip of liquid flow become more and more active with the advantage of drag reduction. Navier linear slip model was confirmed to be available for liquid flow by numerical experiments [15,31,32]. It is convenient to study liquid flow with slip boundary as the accommodation coefficient is related to the slip length accurately. Ahmed [33] applied the BSR method to three-dimensional flow and established an empirical formula of slip length. They tried to find a numerical fitting curve between the accommodation coefficient r and the slip length b. They also discovered that the slip length is independent of shear rate and density, and proportional to the relaxation time. Reis [34] tried to take the first-order Navier–Maxwell slip boundary conditions to simulate slip phenomenon. Švec and Skoçek [35] did further research about the relationship between r and b by a parametric study containing 2000 individual simulations. They claimed that their method is more accurate than Ahmed's method. In fact, two methods are both accurate. The difference in this paper is only the error of interpolation method in calculating slip length. Then, researchers have also tried to link the interaction force at the boundary with the slip boundary condition. For example, Hyväluoma [36] established relationship between the slip length with the interaction force. Wang [37] introduced the adhesion formula for this. But these methods are all empirical. From the above discussion, there are no reliable slip boundary condition for liquid flows in the framework of LBM.

The main challenge to propose slip boundary condition for liquid flow is to create the relationship between slip length and the accommodation coefficient. Inspired by Succi [23] and Guo [25], in this paper, we introduce the half-way and the modified slip boundary conditions from gas flow under the context of LBM. The Navier slip model is adopted to derive the relationship between the accommodation coefficient and the slip length. The rest of the paper is organized as follows: Section 2 describes the numerical method of LBM, and provides the derivation process of the accommodation coefficients. Section 3 is the numerical results and discussion with $2-D$ Couette flow, Poiseuille flow, Water–Cu nanofluid flow, and Womersley flow. Section 4 makes the conclusion.

2. Mathematical and numerical formulation

2.1. Lattice Boltzmann method

The lattice Boltzmann method is a mesoscopic method without the assumption of continuous medium. This method is especially suitable for microscopic flow. Taking advantages of its natural parallelism and ability to handle flexible boundary condition, this study tries to use LBM to simulate laminar liquid flow. The evolution equation can be expressed as [38]

$$f_i(\vec{x}+\vec{e}_i\delta t, t+\delta t) - f_i(\vec{x},t) = -\frac{1}{\tau}\left[f_i(\vec{x},t) - f_i^{(eq)}(\vec{x},t)\right] \tag{1}$$

where $f_i(\vec{x},t)$ is the particle distribution function at the point $\vec{x}$ and the time t, representing the number of particles moving with lattice velocity $\vec{e}_i$, $f_i^{(eq)}$ is the equilibrium particle distribution function (DF), δt is the time step, and τ is the dimensionless relaxation time, which can be expressed as

$$\tau = \frac{\nu}{c_s^2\delta_t} + \frac{1}{2} \tag{2}$$

$$c_s = \frac{c}{\sqrt{3}}; \quad c = \frac{\delta x}{\delta t}$$

where ν is kinematic viscosity, c_s is the sound speed, c is the lattice speed, and δx is the space step. Present study uses the lattice units with $\delta t = 1$ and $\delta x = 1$. In the standard D2Q9 model, the equilibrium distribution function (EDF) can be expressed as [38]:

$$f_i^{eq}(\rho,\vec{u}) = \omega_i\rho\left[1 + \frac{\vec{e}_i\cdot\vec{u}}{c_s^2} + \frac{(\vec{e}_i\cdot\vec{u})^2}{2c_s^4} - \frac{\vec{u}^2}{2c_s^2}\right] \tag{3}$$

where $\vec{u}$ is the macroscopic velocity of fluid, and ρ is the macroscopic density. The lattice velocity $\vec{e}_i$ and the weight coefficient ω_i are given by

$$\vec{e}_i = \begin{cases} (0,0) & i=0 \\ \left(\cos\left[\frac{(i-1)\pi}{2}\right], \sin\left[\frac{(i-1)\pi}{2}\right]\right)c & i=1,2,3,4 \\ \sqrt{2}\left(\cos\left[\frac{(2i-1)\pi}{4}\right], \sin\left[\frac{(2i-1)\pi}{4}\right]\right)c & i=5,6,7,8 \end{cases}$$

$$\omega_i = \left\{1, i=0; \frac{1}{9}, i=1,2,3,4; \frac{1}{36}, i=5,6,7,8.\right.$$

The macroscopic density and velocity are computed by

$$\rho = \sum_i f_i, \quad \rho\vec{u} = \sum_i \vec{e}_i f_i \tag{4}$$

The evolution of the governing equations is divided into two steps. After the collision step, the particle distribution function turns to be $f_i^{'}(\vec{x},t)$. Then, particles stream to next grid, where the particle distribution function turns to be $f_i(\vec{x}+\vec{e}_i\delta t, t+\delta t)$. The program goes into the next loop.

2.2. Boundary condition of LBM for liquid flows with slip

At the beginning, we will introduce two slip boundary conditions, the combined half-way bounce-back condition and half-way specular bounce-back condition method (the half-way method), and the combined modified bounce back condition and modified specular reflection condition method (the modified method) , from gas flow. Fig. 1 shows the boundary grids for the half-way, and the modified methods with the D2Q9 model. In this figure, j is the jth grid, a is the force to drive flow, x is the direction along the flow, and y is the vertical direction. As shown in Fig. 1, for the half-way method, the particle distribution functions f_0, f_1, f_3, f_4, f_7, f_8 can be obtained by stream step, but f_2, f_5, and f_6 are unknown. In the combined half-way bounce-back condition and half-way specular bounce-back condition method (half-way method), the unknown particle distribution functions are given by [23]

$$\begin{aligned} f_2 &= f_4^{'} \\ f_5 &= rf_7^{'} + (1-r)f_8^{'} + 2r\rho\omega_i c_5\cdot u_\omega/2{c_s}^2 \\ f_6 &= rf_8^{'} + (1-r)f_7^{'} + 2r\rho\omega_i c_6\cdot u_\omega/2{c_s}^2 \end{aligned} \tag{5}$$

where u_ω is the velocity of the wall, and r is the accommodation coefficient of the half-way method. Similarly, the unknown distributions f_2, f_5, and f_6 , of the modified method shown in Fig. 1, are treated by [23]

$$\begin{aligned} f_2 &= f_4 \\ f_5 &= r_1 f_7 + (1-r_1)f_8 + 2r\rho\omega_i c_5\cdot u_\omega/2{c_s}^2 \\ f_6 &= r_1 f_8 + (1-r_1)f_7 + 2r\rho\omega_i c_6\cdot u_\omega/2{c_s}^2 \end{aligned} \tag{6}$$

where r_1 is the accommodation coefficient of the modified method. The main challenge to solve above equations is to calculate the accommodation coefficient. For liquid flow, we need to find the relationship between the slip length and the accommodation coefficient. We will do this next.

Then, we derive the relationship between the accommodation coefficient r and the slip length for the half-way method. The lattice on the boundary is shown in Fig. 1. According to the definition of velocity and the stream law of particle distribution function, we can get the function as below [25].

$$u_2 = \frac{1-2\tau+2r(\tau-2)}{1-2\tau+2r(\tau-1)}u_1 + \frac{6(2\tau-1)+r(8\tau^2-20\tau+11)}{(2\tau-1)[1-2\tau+2r(\tau-1)]}a \tag{7}$$

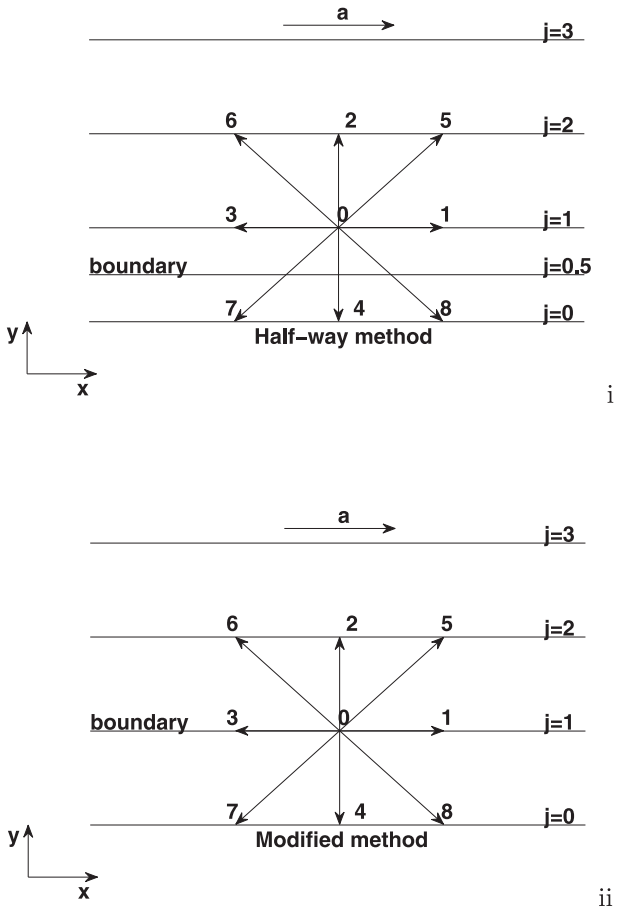

Fig. 1. The boundary grid for (i) half-way method and (ii) modified method with D2Q9 model.

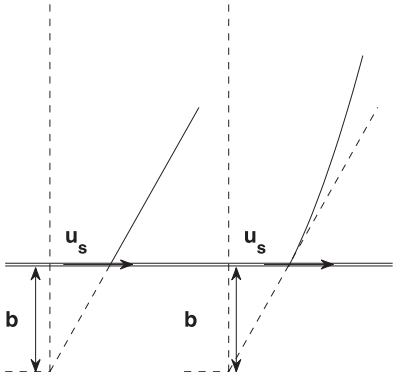

Fig. 2. The sketch of the Navier linear slip model with linear and nonlinear velocity distribution.

where u_1 and u_2 are velocities on the first and second layer grid near boundary. Physically, the linear slip model is given by Eq. (8).

As we know, the Navier linear slip model is proved to be applicable in many case [39,40] (Fig. 2). This model is given by

$$u_s = b\frac{\partial u_j}{\partial y_j} \tag{8}$$

where u_s is the slip velocity, u_j and y_j are the velocity and position of jth layer grid, and b is the slip length, which can be obtained by the test of rheometer. Then, the main work is to present the relation between Eqs. (7) and (8). Eq. (9) displays the sketch of this linear model.

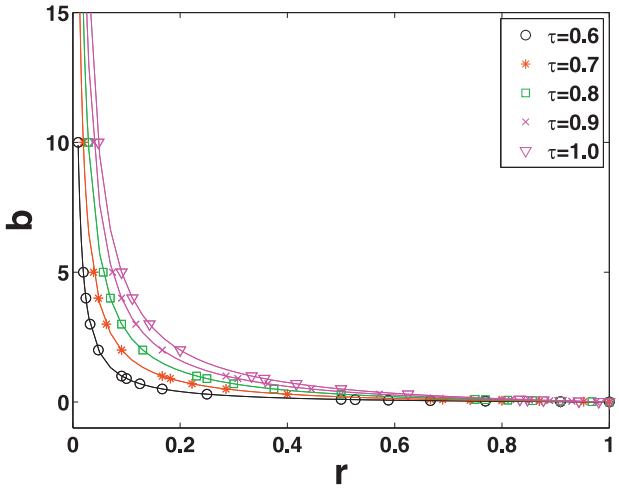

Fig. 3. The relationship between the accommodation coefficient r and the slip length b (in lattice units, the curve is theory data and the discrete points is numerical data).

To derive the relationship between Eqs. (5) and (6), we present an analysis on the internal flow of rheometer. Flow of the rheometer can be simplified as a Couette flow with a driven velocity U. The distance between two plate is h. The velocity distribution function is shown as Eq. (9). The velocity distribution function should satisfy two conditions. The first one is that the slip length is constant. The second one is that the velocity is $u_0 = k_0 U$ for $j = 0$ and the velocity is $u_h = U$ for $j = h$.

$$\begin{aligned} Noslip &: u_j = \frac{y_j}{h}U \\ Slip &: u_j = \frac{y_j}{h}(1-k_0)U + k_0 U \\ k_0 &= \frac{1}{\frac{h}{b}+1} \end{aligned} \tag{9}$$

where k_0 is an intermediate parameter to simplify equations, and y_j is defined as:

$$y_j = (j-0.5)\delta_x \tag{10}$$

Based on the linear slip model of Eq. (8), we can obtain the relationship between the slip length and the slip velocity. With the linear velocity gradient of Couette flow, Eq. (7) can be simplified as:

$$u_2 = \frac{1-2\tau+2r(\tau-2)}{1-2\tau+2r(\tau-1)}u_1 \tag{11}$$

Put Eqs. (9) and (10) into Eq. (11), we get the function of r, which is related to relaxation factor and the slip length.

$$r = \frac{1}{1-\frac{2k_0 h}{\delta_x(1-k_0)(1-2\tau)}} \tag{12}$$

Put the expression of k_0 into Eq. (12), the final form of the equation is Eq. (13)

$$r = \frac{1}{1-\frac{2b}{\delta_x(1-2\tau)}} \tag{13}$$

The relationship between the slip length and the accommodation coefficient is verified in Fig. 3. The curve in the figure is the theory data given by Eq. (13), and the discrete points are the numerical data. The good agreement of the theoretical data and the numerical data indicates the accuracy of this method. Besides,

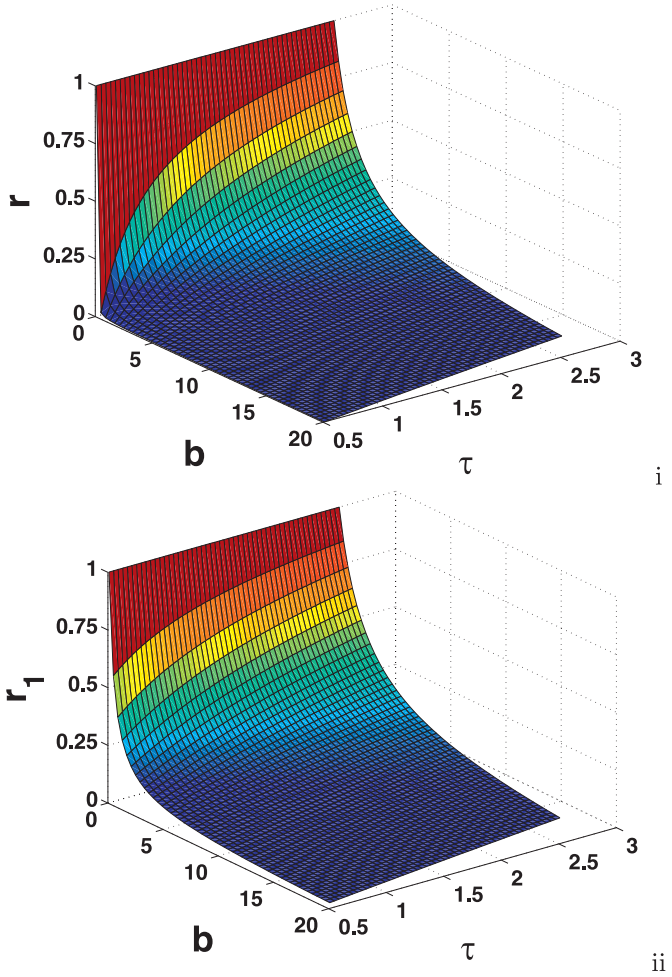

Fig. 4. The display of the accommodation coefficient of the half-way method and the modified method. (i: the half-way method; ii: the modified method.)

the slip length is also sensitive to r when r is smaller than 0.3. When the viscosity is larger, slip length increases with the same accommodation coefficient. Finally, with the same method, the accommodation coefficient r_1 for the modified method can be gotten based on Eq. (6), as shown in Eq. (14).

$$r_1 = \frac{1}{1 + \frac{b}{\tau}} \tag{14}$$

It should be noted that the boundary of the modified method locates at the first layer grid while the boundary of the half-way method has a distance of $0.5\delta_x$ above the first layer grid. The proposed schemes just provide a way to connect the numerical accommodation coefficient with slip length. The numerical stability and the accuracy of the proposed schemes are the same as former works [23,25]. Fig. 4 displays the relationship of the accommodation coefficient, the relaxation factor and the slip length. In the follow section, these schemes are verified with 2-D Couette flow, Poiseuille flow, Water–Cu nanofluid flow, and Womersley flow.

3. Numerical results and discussion

3.1. Linear velocity gradient flows with slip boundary condition

Two slip boundary conditions for liquid flow are introduced in the above section. This subsection verified these schemes with numerical experiment of a 2-D Couette flow. As shown in Fig. 5. the Couette flow is driven by the top plate with a constant velocity $U = 0.09163$. The bottom plate is a stationary wall with slip boundary. The inlet and outlet boundaries are periodic. Without losing generality, $\tau = 0.6$ is used here. *NX* and *NY* are the number of meshes along the direction of x and y respectively. Fig. 6 shows the results of the grid-independent validations for the two slip boundary conditions, indicating that the calculated slip length is very close to the theoretical data with different meshes. The difference between the numerical results and the theoretical data can be hardly observed, even when the meshes is as coarse as 10×10, numerical results show little difference with theoretical data. This is due to the linear velocity distribution of Couette flows. Both the half-way method and the modified method are applicable for liquid flows with linear velocity distribution. To avoid the influence of meshes, we take 100×99(NX $\times$ NY) for the simulation in this subsection. The Reynolds number is equal to 272.1 here.

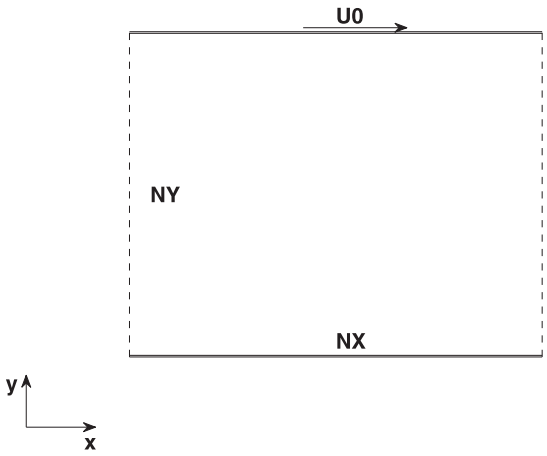

Fig. 5. The computational domain of the 2-D Couette flow.

Then, we also studied the influence of the gap between the up and bottom plates. Figs. 7 and 8 show the velocity distributions of the Couette flows with the two slip boundary conditions for the slip length $b = 0.5$ and $b = 5.5$, respectively. u is the velocity along the direction of x. Although the slip velocities vary with the height of the gaps, the slip lengths keep the same. This means the slip length is independent of the shear rate. This conclusion is consistent with the result in previous works [37,41].

The influence of driven velocity was also discussed below. As we know, the Mach number must be less than 0.3 for an incompressible flow. We took five driven velocities to verify the stability of the two slip boundary conditions with different Mach numbers. As shown in Figs. 9 and 10, numerical results indicate that the proposed boundary conditions are reliable when Mach number is less than 0.3. The slip length is constant regardless of the change of the driven velocity. It can be concluded that the velocity gradients have little effect on boundary slip phenomenon.

3.2. Non-linear velocity gradient flows with slip boundary

As discussed above, the proposed boundary conditions are available for linear velocity gradient flows. In this part, we verified the application of these two methods for flows with nonlinear velocity gradient. Poiseuille flow is studied in this subsection. As shown in Fig. 11, the top plate and the bottom plate are walls with slip boundary. The inlet and outlet boundaries are periodic. The fluid domain is driven with a constant body force, a. The velocity distribution of Poiseuille flow is presented as follows.

$$u_j = 4u_{max} \cdot \frac{y_j}{h}\left(1 - \frac{y_j}{h}\right) \tag{15}$$

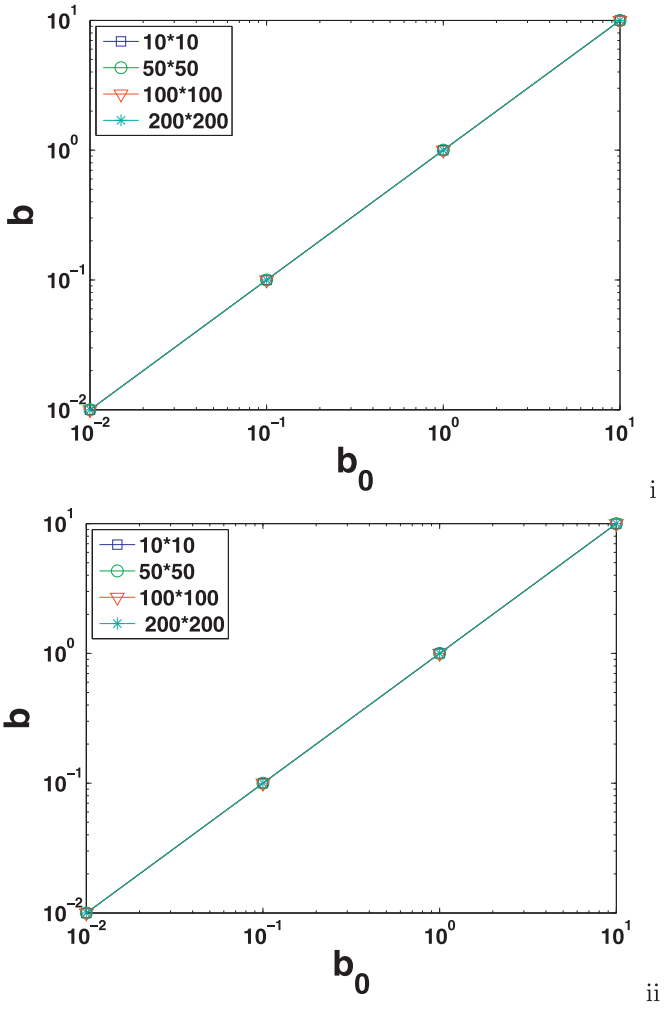

Fig. 6. Grid-independent validations of the 2-D Couette flow. b_0 is the physical slip length and b is the slip length by numerical methods. (i:the half-way methods; ii:the modified method.)

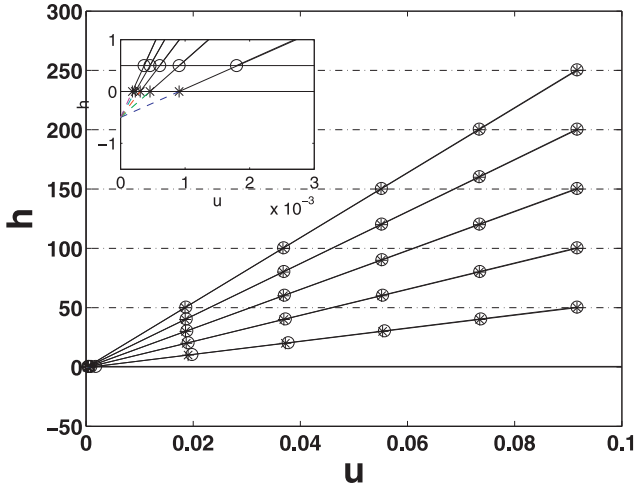

Fig. 7. The velocity distributions with different gaps (gaps(h) are 50,100,150,200,250. o is the data with the half-way method and * is the data with the modified method, $b = 0.5$).

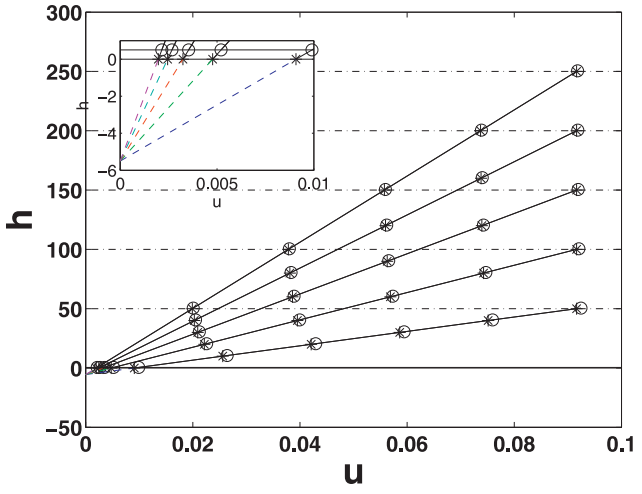

Fig. 8. The velocity distributions with different gaps (gaps(h) are 50,100,150,200,250. o is the data with the half-way method and * is the data with the modified method,$b = 5.5$).

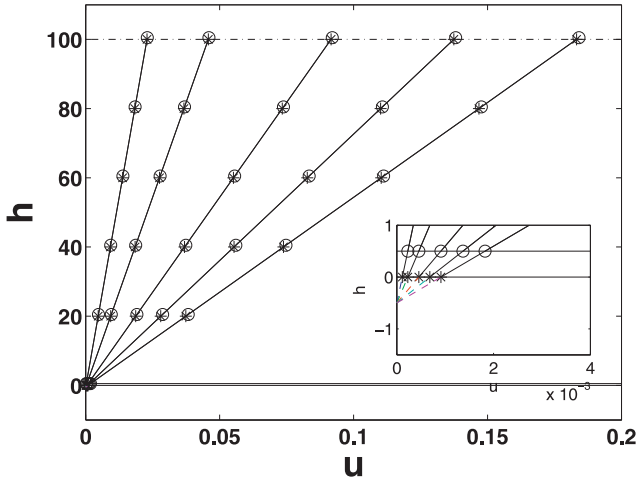

Fig. 9. The velocity distributions with different driving velocities (driven velocities are 0.25U, 0.5U, 1.0U, 1.5U, 2.0U. o is the data with the half-way method and * is the data with the modified method, $b = 0.5$).

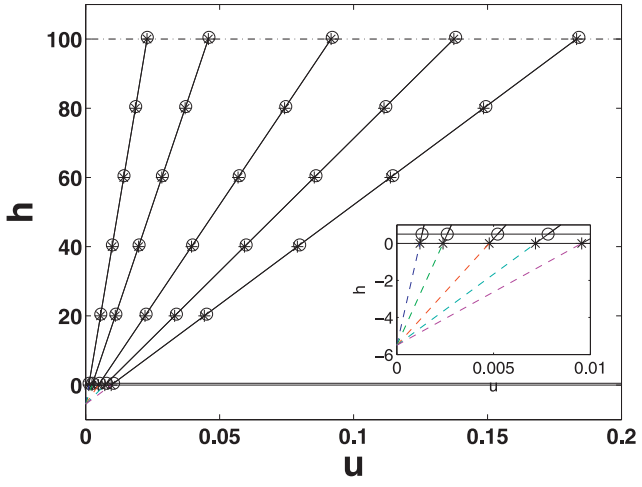

Fig. 10. The velocity distributions with different driving velocities (driven velocities are 0.25U, 0.5U, 1.0U, 1.5U, 2.0U. o is the data with the half-way method and * is the data with the modified method, $b = 5.5$).

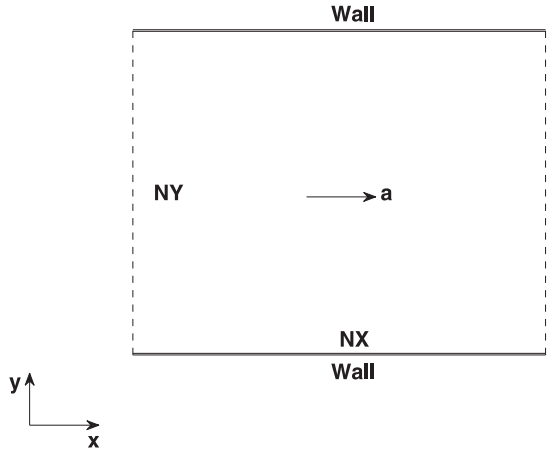

Fig. 11. The computational domain of the 2-D Poiseuille flow.

$$u_j = 4u_{max} \cdot \frac{y_j}{h}\left(1 - \frac{y_j}{h}\right) + u_s$$

$$u_{max} = \frac{ah^2}{8\nu} \tag{16}$$

where u_{max} is the maximum velocity along the center line of the channel and h is the gap of the channel. With the definition of Reynolds number in Eq. (17), the Reynolds number varies from 29.4 to 1058.8 for Poiseuille flow in this subsection.

$$Re = \frac{h \cdot u_{max}}{\nu} \tag{17}$$

Clearly, we can see that the three main factors affecting the flow field of the Poiseuille flow with slip boundary, are the slip length (b), the relaxation factor (τ), and the body force (a). For 2-D Poiseuille flows, Eq. (15) is applied to replace Eq. (9). With the method in the above section, we can get accommodation coefficient of the half-way method and the modified method for 2-D Poiseuille flows, which is expressed as follows.

For the half-way method:

$$r = \frac{1}{1 + \frac{b + (\frac{1}{4} - \frac{2}{3}(\tau - 0.5)^2)\Delta}{\tau - 0.5}}$$

$$b_{error} = \left(\frac{1}{4} - \frac{2}{3}(\tau - 0.5)^2\right)\Delta \tag{18}$$

For the modified method:

$$r_1 = \frac{1}{1 + \frac{b - \frac{1}{6}(8\tau^2 - 2\tau - 1)\Delta}{\tau}}$$

$$b_{error} = \frac{1}{6}(8\tau^2 - 2\tau - 1)\Delta \tag{19}$$

where $\Delta = \delta_x/NY$ is related to the number of meshes. Compared with Eqs. (13) and (14), an error term, b_{error}, is added in above equations, which is associated with meshes and the relaxation factor. Fig. 12 shows the error curves of the accommodation coefficients for the half-way and the modified method. The absolute value of the error term of the modified method increases as the increase of the relaxation factor. As to the half-way method, when the relaxation factor is smaller than 1.11, the absolute value of the error term decreases as the increase of the relaxation factor, in contrary to the situation when the relaxation factor is bigger than 1.11. When the relaxation factor is less than 0.68, the error of the modified method is smaller than that of the half-way method. Otherwise, the error of the modified method is larger. In practice, the relaxation factor is usually smaller than 2.0. If the

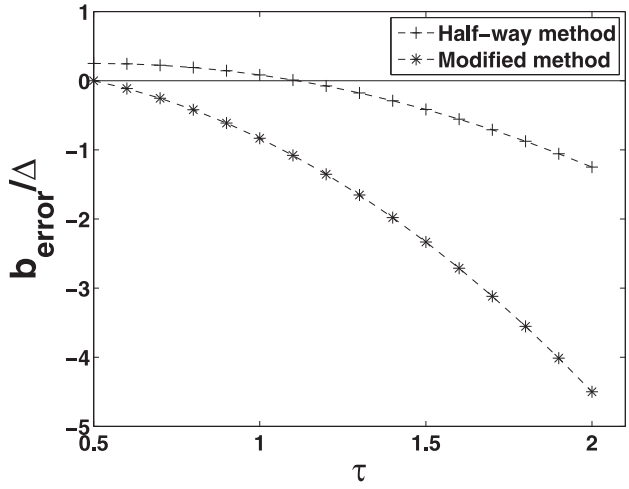

Fig. 12. The error terms of the accommodation coefficient.

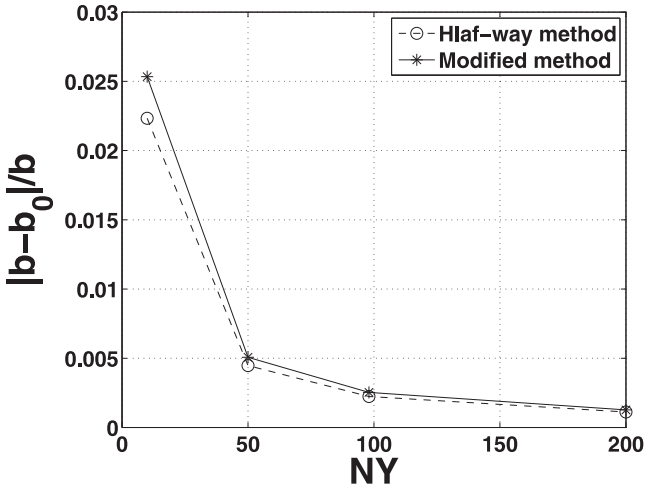

Fig. 13. Grid-independent validations of the 2-D Poiseuille flow ($b_0 = 1.0$ and $\tau = 0.7$).

mesh of the channel is fine enough, the error term is ignorable. Thus, Eqs. (18) and (19) are simplified to Eqs. (13) and (14), which can be applied to non-linear velocity gradient flows. As shown in Fig. 13, $NY = 98$ is fine enough for the following simulations. In simulations, meshes are 100×98, where Δ is about 0.01. So the error for slip length is less than 0.0108 with the applying of Eqs. (18) and (19).

Figs. 14 and 15 display the horizontal velocity profiles of the Poiseuille flow with different slip length (b), relaxation factor (τ), and body force (a), for the half-way and the modified method respectively. In these figures, the slip length is set to be 0, 1.0, 3.0 in lattice units. Fig. 16 is the comparison of the halfway method with the modified method with large slip length. The points are the numerical results where the dash lines are the theoretical data of Eq. (15). It is clear that the numerical results agree well with the theoretical solution. At point y_i, velocity of flows with slip is larger than that without slip with the same relaxation factor and the body force, and the difference of velocity between slip model and no-slip model is constant at any point, which agrees with the theoretical solution. When the relaxation factor or the body force changes, u_s changes correspondingly. But the slip length is still equal to the setting data. If the relaxation factor becomes larger, u_s becomes larger which is consistent with the linear slip model.

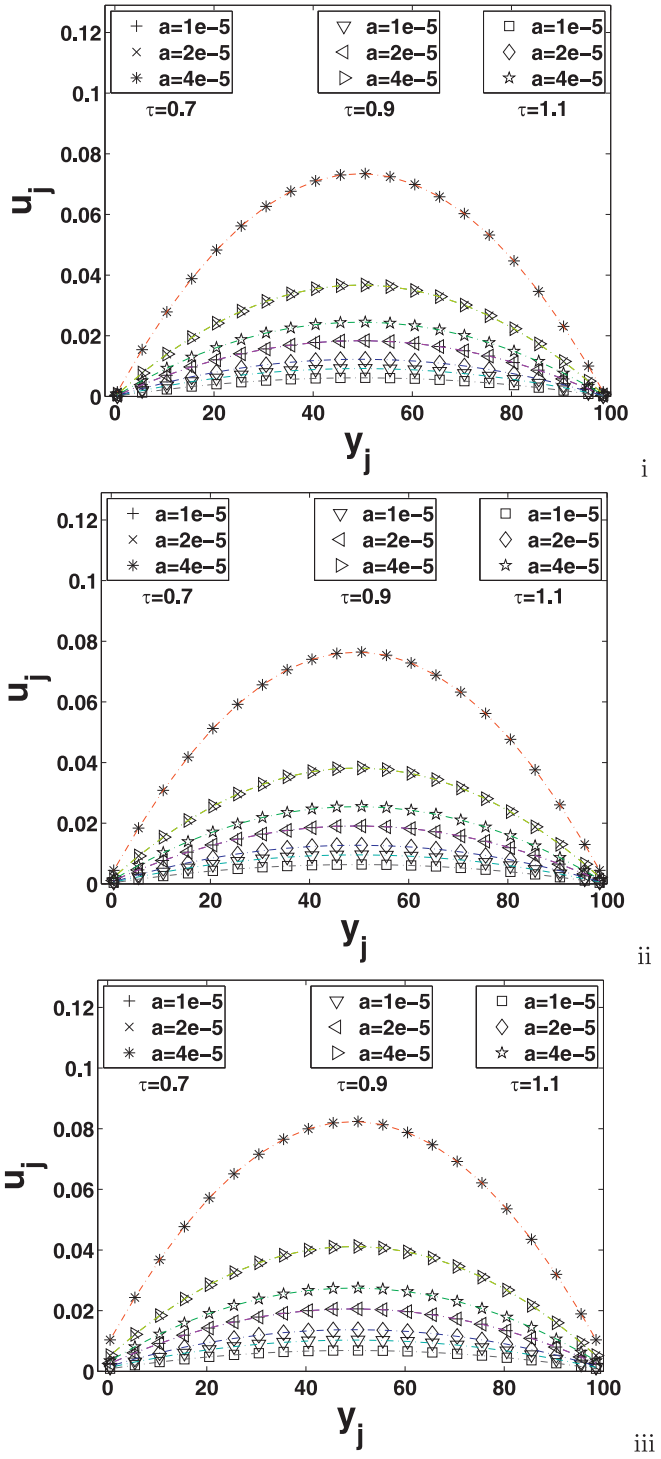

Fig. 14. Horizontal velocity profiles of the Poiseuille flow with slip boundary. The points are the numerical data with the half-way slip boundary while the dash lines are the theory data. (The slip lengths are respectively 0(i), 1.0(ii), 3.0(iii).)

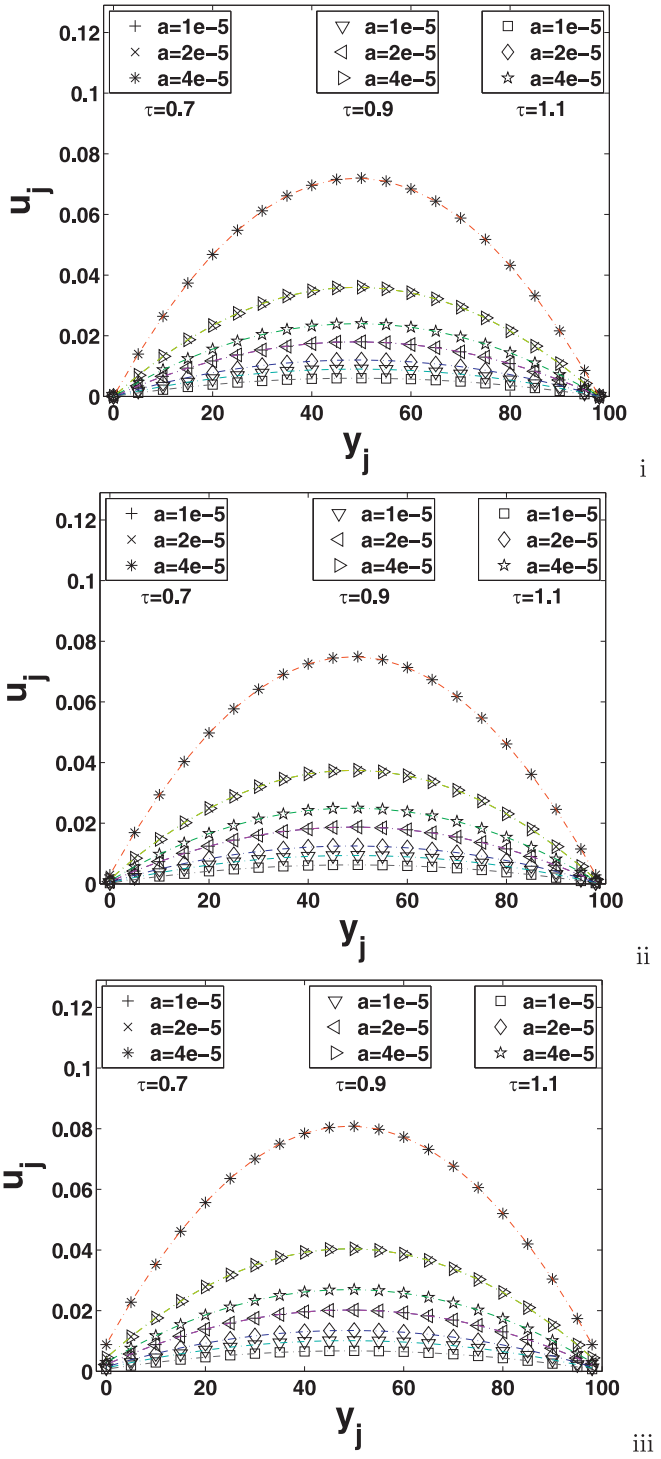

Fig. 15. Horizontal velocity profiles of the Poiseuille flow with slip boundary. The points are the numerical data with the modified slip boundary while the dash lines are the theory data. (The slip lengths are respectively 0(i), 1.0(ii), 3.0(iii).)

In addition, with the increment of the slip length, velocity distributions are almost the same except that the velocities on the boundary become larger. Large driven force and small viscosity result in large velocity. The velocity distribution of the channel with the conditions $\tau = 0.7(\nu = 0.066667), a = 1e-5$ and $\tau = 0.9(\nu = 0.133333), a = 2e-5$ are extremely consistent with Eq. (15). This consistency indicates the accuracy of the slip boundary conditions proposed in this study. The question remains on why the boundary condition based on the linear velocity distribution can be applied to the non-linear flow.

We can give a brief analysis. The linear velocity gradient hypothesis is only applied in the first and the second layer grid. The calculation of real slip length requires the slope of velocity distribution at the first layer grid. If the grid is fine enough, the slope is nearly equal to the difference of velocity of the first and the second layer grid. For more complex flows, these slip boundary

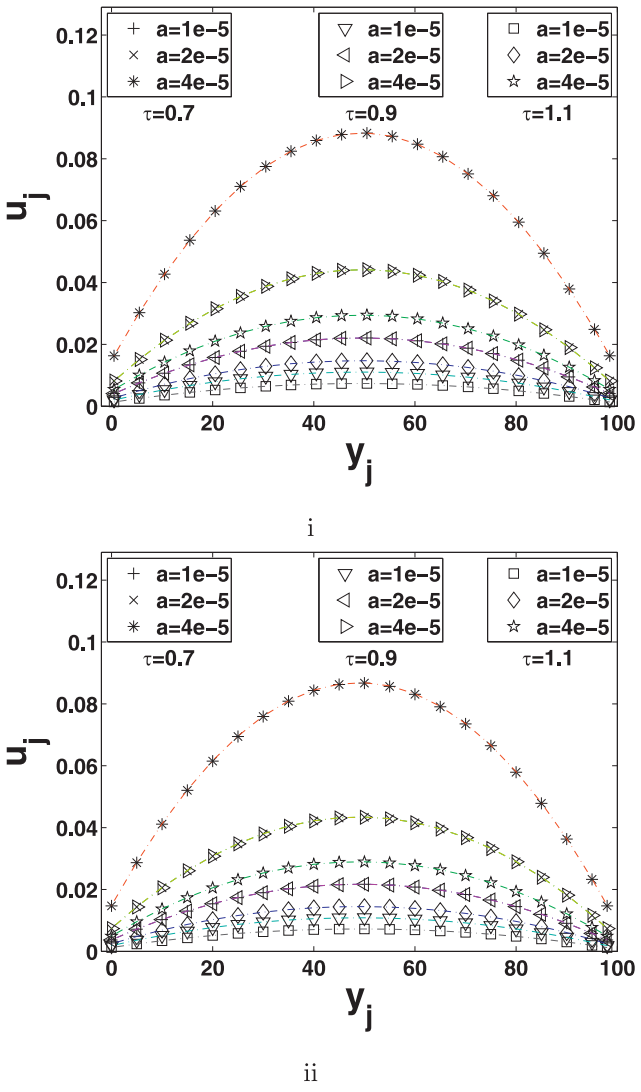

Fig. 16. Horizontal velocity profiles of the Poiseuille flow with large slip length ($b = 5.0$). The points are the numerical data with the modified slip boundary while the dash lines are the theory data (i:Half-way method; ii:Modified method).

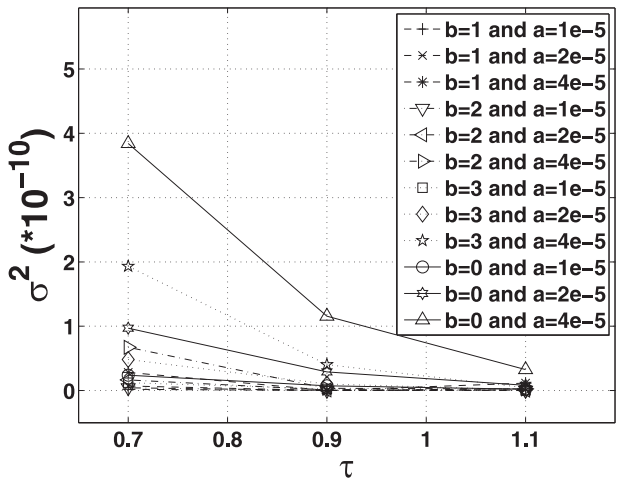

Fig. 17. The relative error of velocity distributions of the Poiseuille flow with the half-way method.

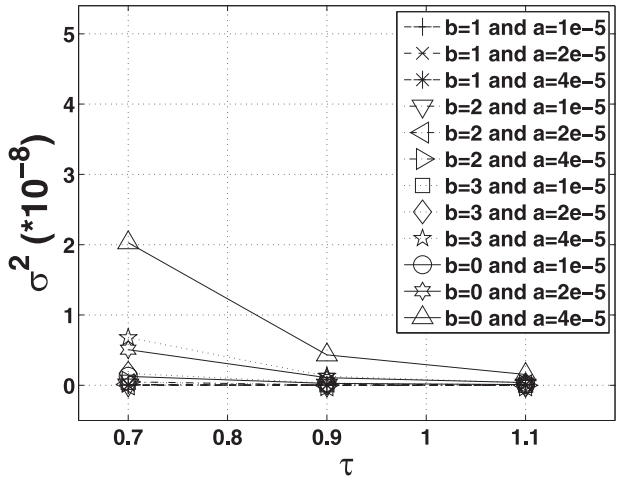

Fig. 18. The relative error of velocity distributions of the Poiseuille flow with the modified method.

conditions are still applicable as long as the grid is fine enough. It should be noted that these two methods will result in loss of accuracy when applied to flows with non-linear velocity gradient. We take Eq. (20) to measure the accuracy of the proposed methods.

$$\sigma^2 = \frac{\sum_{j=0}^{NY}(u_j - u_t)^2}{NY} \tag{20}$$

where u_j is the velocity of the numerical data, and u_t is the velocity of the theoretical data at the same point. As shown in Figs. 17 and 18, both two methods are very accurate for the Poiseuille flow. These relative errors for the Poiseuille flow are larger than the Couette flow. The calculation of the slip length requires the information of the velocity gradient on the boundary. Second order linear interpolation is applied to calculate the slip velocity and the velocity gradient.

For the half-way method:

$$\begin{aligned} u_s &= u_{0.5} = \frac{15}{8}u_1 - \frac{5}{4}u_2 + \frac{3}{8}u_3 \\ \frac{\partial u_j}{\partial y_j}\,|_{y_i=0.5} &= -2u_1 + 3u_2 - u_3 \end{aligned} \tag{21}$$

For the modified method:

$$\begin{aligned} u_s &= u_1 \\ \frac{\partial u_j}{\partial y_j}\,|_{y_i=1} &= -\frac{3}{2}u_1 + 2u_2 - \frac{1}{2}u_3 \end{aligned} \tag{22}$$

For the half-way method, we do not have the information of velocities on the boundary. So we use extrapolation method to get the velocity gradient on the boundary with the half-way method, which is shown in Eq. (21). For the modified method, velocities on the boundary are known. So, interpolation method is used to calculate the slip length with velocity distribution, which is shown in Eq. (22). Therefore the modified method is more appropriate for flows with higher accuracy requirement on the slip length and the boundary velocity gradient.

3.3. Applying to water–Cu nanofluid flow

Laminar forced convection of nanofluids in a microchannel is a classic case attracting lots of attention. With slip velocity on the channel walls, the velocity profile has much difference with the nonslip one. Karimipour [10–12] focuses on the mass

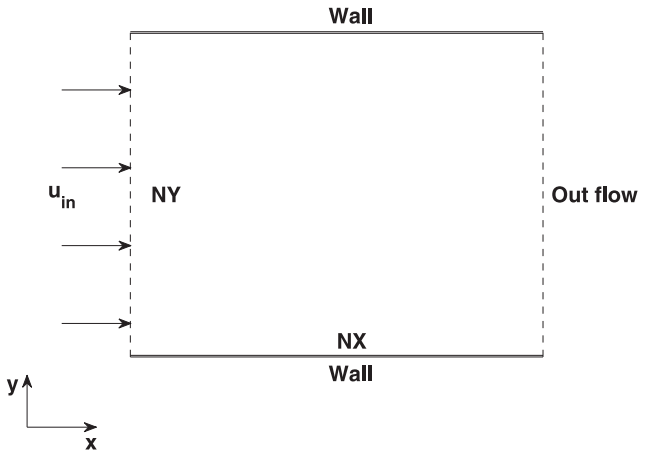

Fig. 19. The computational domain of the water–Cu nanofluid flow.

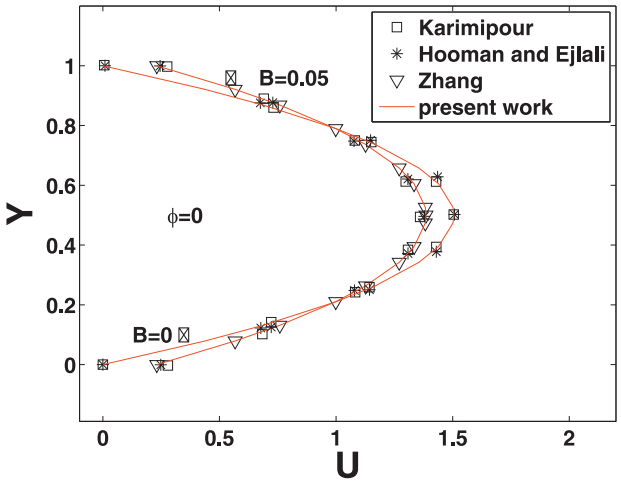

Fig. 20. Comparison of the normalized fully developed velocity profiles with Karimipour [12], Hooman [42], and Zhang [43].

transportation of water–Cu nanofluid flows in a microchannel with slip boundary. They used an approximate method to get the accommodation coefficients. This subsection tried to simulate the water–Cu nanofluid flow with accurate accommodation coefficients provided by the proposed methods in current study. We analyzed the velocity field of flows with slip boundary. As shown in Fig. 19, the top plate and the bottom plate are walls with slip boundary. The inlet is velocity boundary with U and the outlet is out flow boundary condition. Water–Cu nanofluid is a homogeneous mixture of water and Cu nanoparticles, with an effective density obtained by:

$$\rho_{mix} = (1-\varphi)\rho_{water} + \varphi\rho_{Cu}$$
$$\rho_{water} = 997.1\ \mathrm{kg/m^3};\ \rho_{Cu} = 8954\ \mathrm{kg/m^3} \tag{23}$$

where φ is the nanoparticle volume fraction. The effective dynamic viscosity is expressed by [44]:

$$\mu_{mix} = \mu_{water}/(1-\varphi)^{2.25}$$
$$\mu_{water} = 8.91 \times 10^{-4}\mathrm{Pa}\cdot\mathrm{s} \tag{24}$$

The parameters of this simulation are dimensionless, which is assigned as:

$$U = u/u_{in}$$
$$B = b/h$$
$$Y = y_i/h \tag{25}$$

A lattice of 800×40 nodes is applied , which is the same as Karimipour [12]. Re is 0.01. The inlet is a uniform velocity, u_{in}, while the outflow is free flow. L is the length of the channel. The modified slip boundary was used at upper and bottom walls. The numerical accommodation coefficient was calculated by Eq. (14). Simulations were performed with nanoparticle volume fractions (φ) from 0 to 0.04 and slip length (B) from 0.005 to 0.02. Fig. 20 shows the comparison of the normalized fully developed velocity profiles with many researchers for $B = 0.00$ and $B = 0.05$. This case is used for the validation with pure water, $\varphi = 0$. When $B = 0.00$, present data agrees well with simulations by Karimipour [12], Hooman [42]. This is because that slip boundary with $B = 0.00$ is equal to non slip boundary, and the numerical accommodation coefficient is 1. When $B = 0.05$, the non-dimensional slip length calculated with numerical velocity profiles in present work is 0.05008, which agrees better with the setting data than the simulations by Karimipour [12], Hooman [42], and Zhang [43]. This is because the accommodation coefficients of other methods are chosen approximatively.

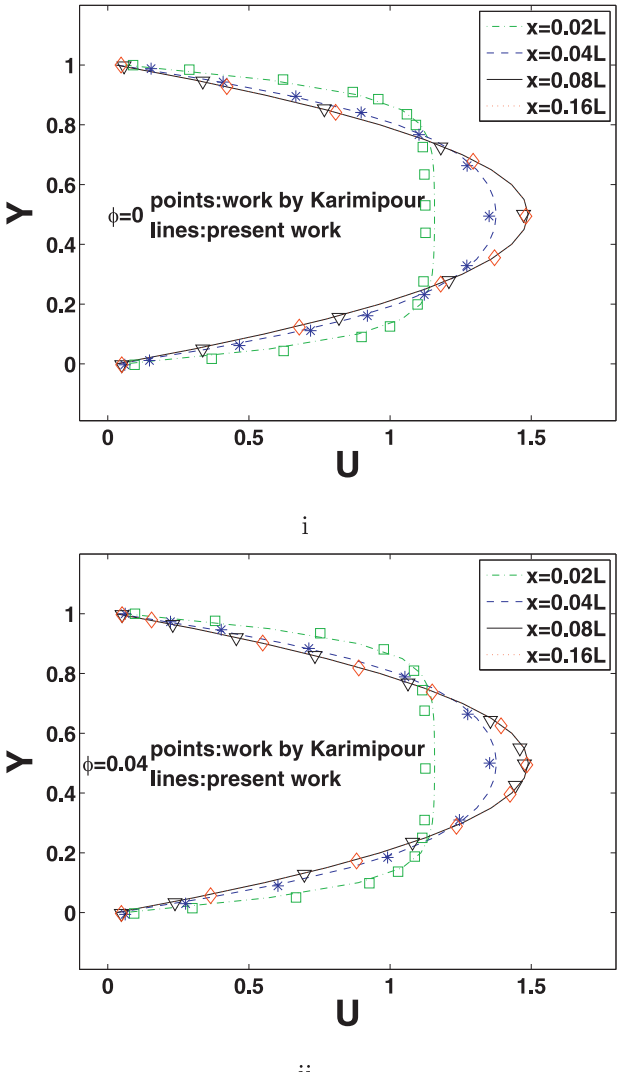

Fig. 21. Horizontal dimensionless velocity profiles along the microchannel with $B = 0.005$ for $\varphi = 0$(i) and $\varphi = 0.04$(ii). Points are the data by Karimipour [12].

Table 1
Slip length for water–Cu nanofluid flows ($\varphi = 0.04$).

B	Karimipour [12]	Present
0.005	0.00870	0.00505
0.01	0.0132	0.01005
0.02	0.0245	0.02005

Fig. 21 shows the horizontal dimensionless velocity profiles along the microchannel with $B = 0.005$ for $\varphi = 0$ and $\varphi = 0.04$. $x = 0.02L$ and $x = 0.04L$ are the short entrance length near the inlet. Velocity profile is fully developed soon after the entrance, at $x = 0.08L$ and $x = 0.16L$. It can be obtained that the Cu particles volume fraction makes little difference to velocity profile. The theoretical analysis verifies this conclusion which is shown as follows. The conservation of mass for an incompressible viscous flow can be expressed by:

$$\int_0^1 U_{X=X_0} dY = \int_0^1 U_{in} dY \tag{26}$$

With Eqs. (8), (15), and (26), we can calculate the slip velocity of this case. When flows are fully developed, with $U_s = u_s/u_{in}$ and $U_c = u_c/u_{in}$, the non-dimensional form of slip velocity is

$$\frac{2}{3}U_c + U_s = 1 \tag{27}$$

$$U_s = 4BU_c \tag{28}$$

With this equation, the slip velocity has nothing to do with the particles volume fraction. If $B = 0.005$, the slip velocity is 0.029126. The slip velocity in simulation is 0.029572 for $\varphi = 0$ and 0.029516 for $\varphi = 0.04$, which shows good agreements with analyzed data. The effect of the slip length B is also examined. Fig. 22 shows the horizontal dimensionless velocity profiles U along the microchannel with $\varphi = 0.04$ for $B = 0.01$ and $B = 0.02$. It can be obtained that larger B results in larger slip velocity.

The slip length in Table 1 is calculated by the velocity distribution where $x = 0.16L$. As discussed in the above subsection (Eq. (19)), the error of the slip length with the modified method is only related to the mesh and the relaxation factor, not the slip length, which can be verified by the present data. How to choose accommodation coefficient is the main factor affecting simulation results. From Table 1, we can conclude that present data is more accurate than the data by Karimipour [12]. Present slip boundary is suitable for non-linear velocity gradient flows with fine enough meshes.

3.4. Applying to unsteady flow: 2-D Womersley flow

The proposed schemes rely on the theoretical solution of the slip velocity in different flow configurations, which shows good agreement with the previous researches and the theoretical data in the above subsections. Simulation of more complex liquid flow with high Reynolds number can verify the generality of the proposed slip boundary condition. Thus, a two-dimensional Womersley flow (pulsatile flow in two-dimensional channel) [45,46] is employed. The geometric configuration of the Womersley flow is identical to that of the Poiseuille flow, while the flow is driven by a periodic pressure gradient instead of a constant one.

$$\frac{\partial P}{\partial x} = Real[ae^{i\omega t}] \tag{29}$$

where a is the amplitude, ω is the frequency, t is the variable of time, i is the symbol of imaginary number. Real means the real

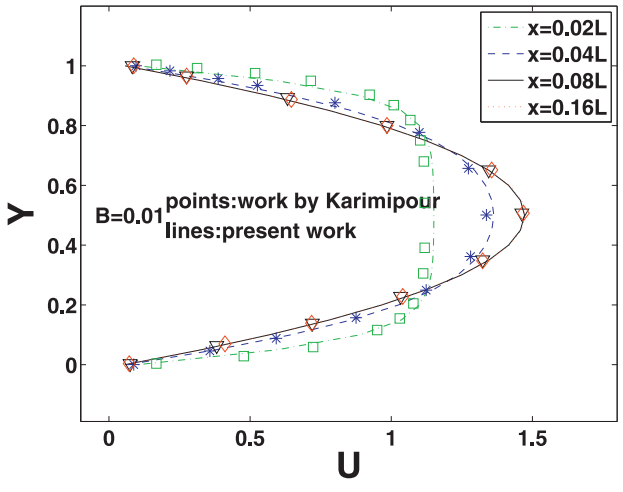

i

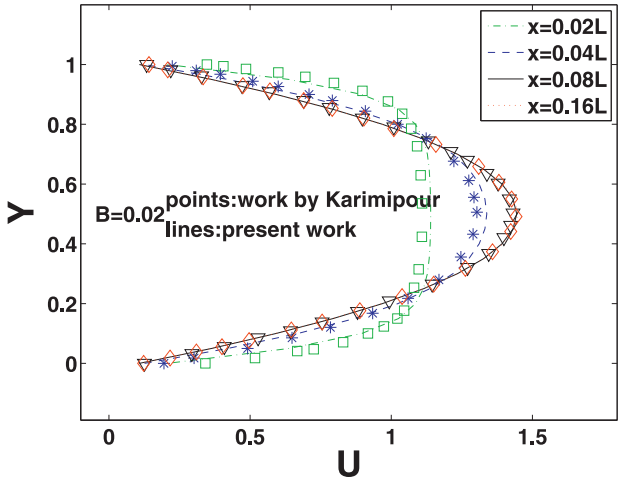

ii

Fig. 22. Horizontal dimensionless velocity profiles along the microchannel with $B = 0.01$(i) and $B = 0.02$(ii) for $\varphi = 0.04$. Points are the data by Karimipour [12].

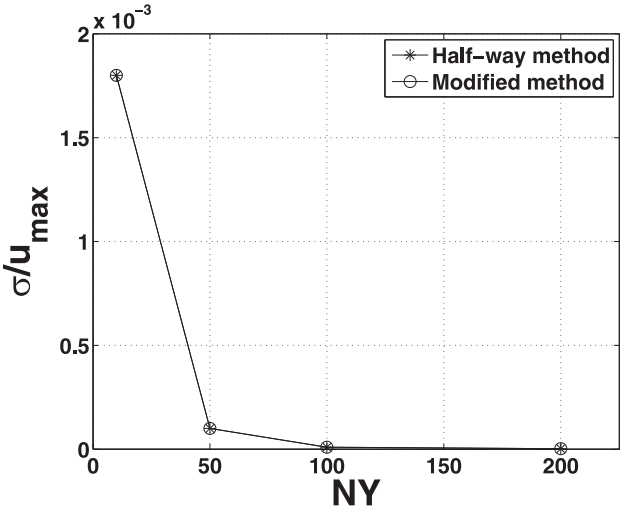

Fig. 23. Relative error of the velocity distributions for the Womersley flow with non-slip boundary ($Re = 100$; $Wo = 4$).

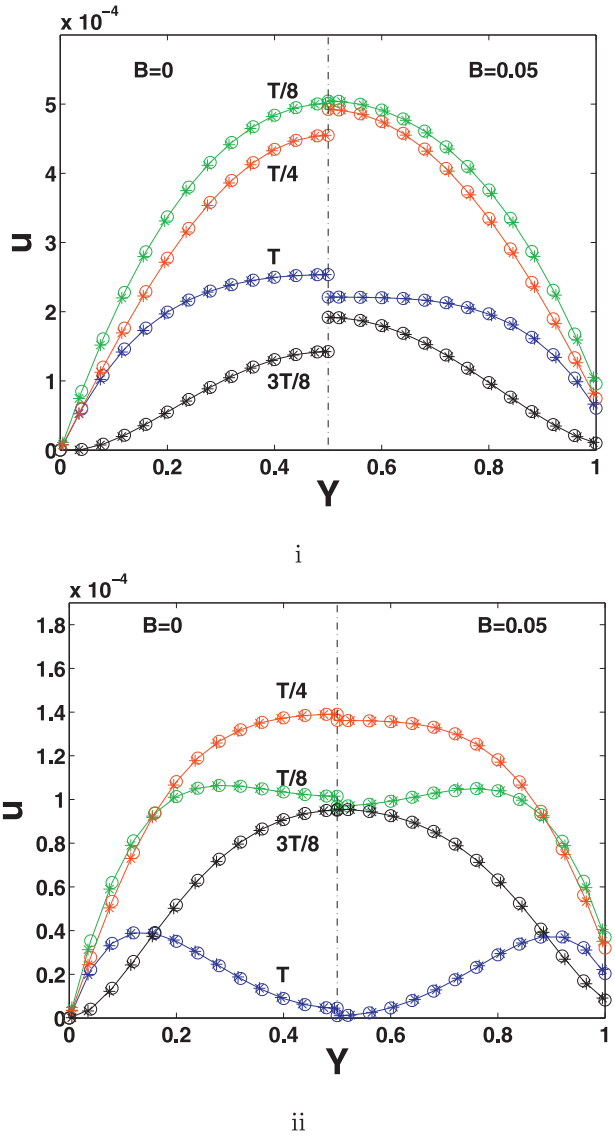

Fig. 24. Horizontal velocity profiles along the channel of the Womersley flow with different Womersley numbers. The Reynolds number is constantly equal to 100 (i:Wo = 2.0; ii:Wo = 4.0. o is the numerical data with the half-way method; * is the numerical data with the modified method; lines are the theoretical data).

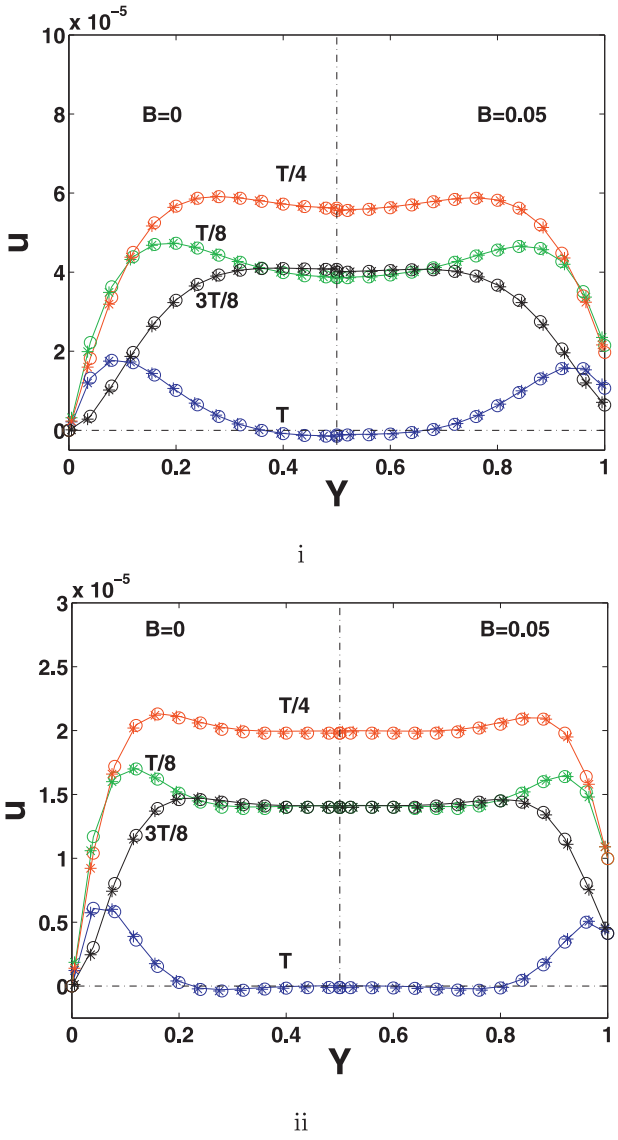

Fig. 25. Horizontal velocity profiles along the channel of the Womersley flow with different Womersley numbers. The Reynolds number is constantly equal to 100 (i:Wo = 6.0; ii:Wo = 10.0. o is the numerical data with the half-way method; * is the numerical data with the modified method; lines are the theoretical data).

part, and $\partial P/\partial x$ is the periodic pressure gradient. In simulations, the periodic pressure gradient can be treat as a periodic body force. The frequency can be expressed as $\omega = 2\pi/T$. T is the period of the driving pressure. The solution of the Navier–Stokes equation with non-slip boundary is [45,46]:

$$u_j = Real\left[i\frac{a}{\omega}\left(1 - \frac{\cos(\lambda(2Y-1))}{\cos(\lambda)}\right)e^{i\omega t}\right] \tag{30}$$

where Y is the dimensionless distance of the channel, defined as $Y = y_j/h$, and λ is given in terms of the Womersley number, W_o, which is defined as:

$$\lambda^2 = -iW_0^2, W_0^2 = \frac{\omega h^2}{4\upsilon} \tag{31}$$

With the slip boundary of Eq. (8), the analytical solution for the velocity in this case is given by:

$$u_j = Real\left[i\frac{a}{\omega}\left(1 - \frac{\cos(\lambda(2Y-1))}{\cos(\lambda) - 2B\lambda\sin(\lambda)}\right)e^{i\omega t}\right] \tag{32}$$

At first, we took the non-slip Womersley flow to study grid independence with constant Reynolds number, 100, and Womersley number, 4.0. The definition of Reynolds number is the same as Eq. (17) in Section 3.2. In this subsection, the kinematic viscosity is equal to 0.001.

Eq. (20) was taken to calculate the error between the numerical and the theory data. With periodicity of flows, average error at time T, $T/8$, $T/4$, $3T/8$ can represent the error of the total period. Ten periods are calculated to ensure stability. The data of the 10th period is presented here. As shown in Fig. 23, the error of the velocity distributions decrease as the number of grids increases. When the mesh is larger than 100×100, the error can be ignorable. Therefore the following numerical experiments were studied with meshes of 100×100. To verify the generality of the proposed slip boundary condition, the Womersley flow is studied with various Womersley numbers. The Reynolds number in these cases is constantly 100. Half of the computational domain is presented in figures because of the symmetry of the velocity distributions

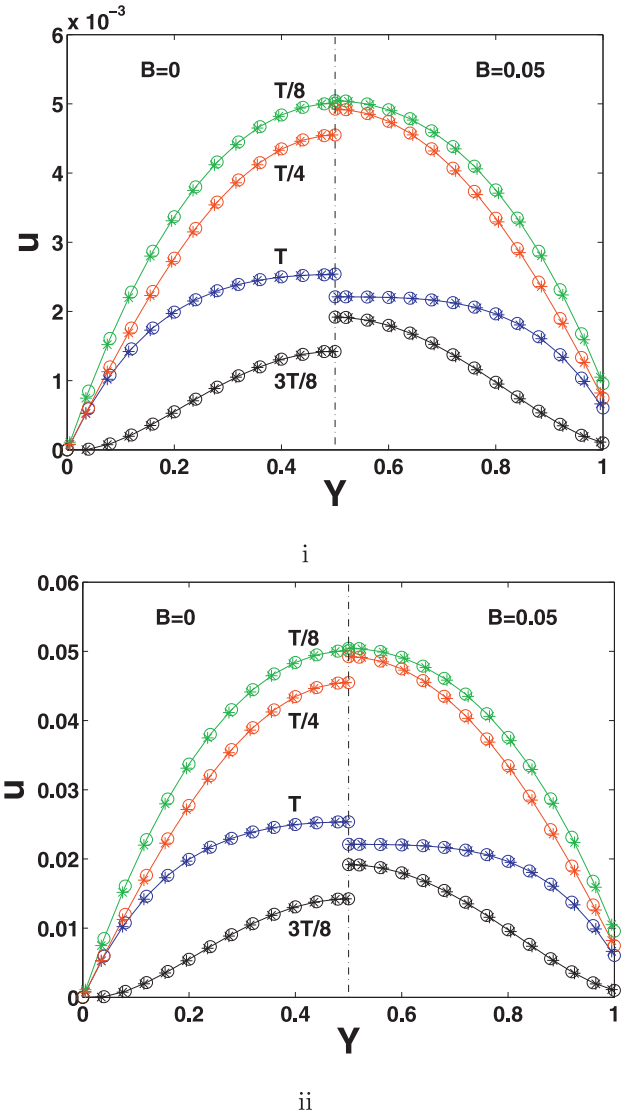

Fig. 26. Horizontal velocity profiles along the channel with $B = 0$ and $B = 0.05$ of the Womersley flow with different Reynolds numbers (i:$Re = 1000$; ii:$Re = 10{,}000$. o is the numerical data with the half-way method; * is the numerical data with the modified method; lines are the theoretical data).

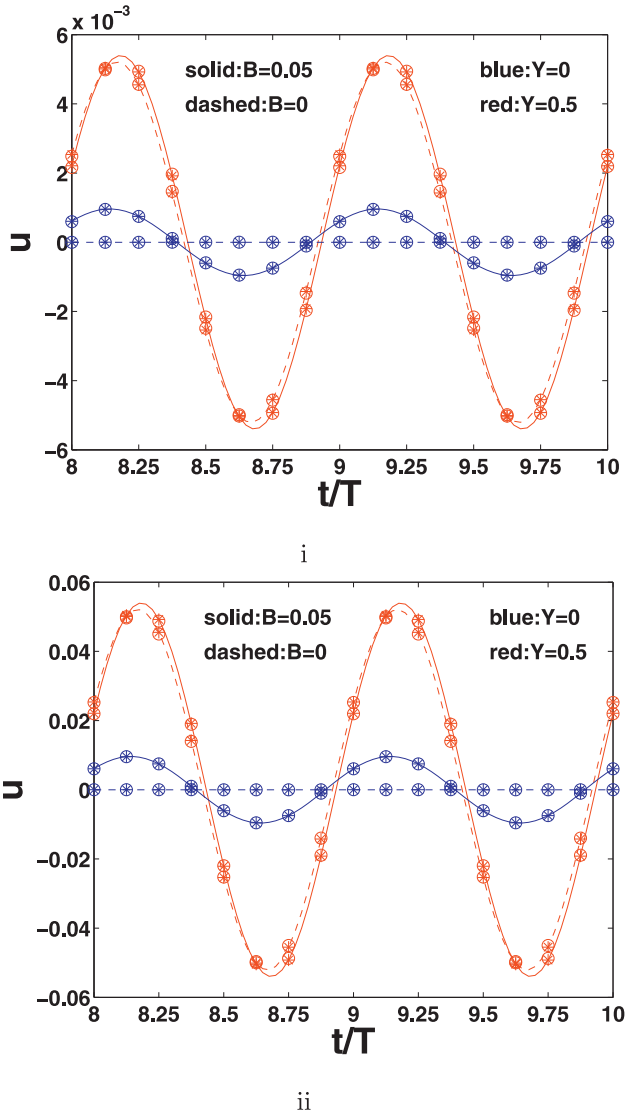

Fig. 27. Time domain of velocity at different position in the channel of Womersley flow with $B = 0$ and $B = 0.05$ (i:$Re = 1000$; ii:$Re = 10{,}000$. o is numerical data with half-way method; * is numerical data with modified method; lines are theoretical data).

along the y direction. In Figs. 24 and 25, the numerical data is consistent with the theoretical data. Both the half-way method and the modified method have the same accuracy in simulating the Womersley flow. When the slip length is equal to zero, the velocity on the boundary is zero at any time T. The velocity on the boundary changes along time where there exists a slip length. For flows with $Wo = 6.0$ and $Wo = 10.0$ in Fig. 25, the velocity distribution near the boundary is strong nonlinear. The good agreement of the numerical and the theoretical data in this case indicates the generality of the proposed slip boundary conditions.

Then, simulations of the Womersley flow with different Reynolds numbers are implemented to verify the application of the proposed slip boundary conditions on high speed flows. For LBGK method, the Mach number must be less than 0.3, which is defined as $Ma = u/c_s$. With this limitation, two cases with $Re = 1000$ and $Re = 10,000$ are experimented, as shown in Fig. 26. The Womersley number is equal to 2.0. Compared with the flow with $Re = 100$ in Fig. 24, the speed has little effect on the accuracy of the proposed slip boundary conditions.

For Womersley flow, the slip boundary has little effects on the flow at the center of the channel while it significantly affects the flow near the boundary. In Fig. 27, the time domain of velocity is slightly different between numerical data with and without slip boundary at the position Y = 0.5 while it is extremely different at the position Y = 0. The slip velocity on the boundary is associated with the velocity gradient with Eq. (8). For unsteady flow, slip velocity changes with time.

In this subsection, 2-D Womersley flows were applied to study the generality of the proposed slip boundary condition. we can conclude from the above discussions that the proposed slip boundary conditions are applicable for non-linear flows.

In above subsections, the proposed schemes are verified to be applicable for laminar liquid flow with slip boundary. These schemes remains to be verified for turbulence flow. There are two difficulties to apply these method to turbulent flows. The first one is the large amount of calculation. The second one is that the hypothesis of the linear slip model may break down for turbulent flows. Extending the slip boundary conditions to turbulent flows will be our further work.

4. Conclusion

In this paper, two slip boundary conditions, the half-way method and the modified method, have been discussed to simulate liquid flows with slip boundary. Based on the hypothesis of the Navier linear slip model, the accommodation coefficients are firstly developed by theoretical derivation for liquid flows. With the analysis of the numerical data for 2-D Couette flows and Poiseuille flows, we can conclude that the proposed schemes are particularly suitable for liquid flows with linear and non-linear velocity gradient. The numerical results with these boundary conditions are almost identical to the theoretical solutions. Moreover, the applying of the present work to water–Cu flows shows advantages compared with the former researches. The proposed methods are more accurate than the approximately choosing accommodation coefficients in former works. Finally, simulations of 2-D Womersley flows can verify the generality of the proposed slip boundary conditions. For flows with nonlinear velocity distributions, the error of the modified method is less than that of the half-way method when the relaxation factor is less than 0.68. Otherwise, the error of the modified method is larger. However, the precise slip velocity on the boundary is provided with the modified method while the extrapolation method is taken to calculate the slip velocity with the half-way method. If the focus is the center field of flow, the half-way method is better in many cases. If the focus is the field near the boundary, the modified method is more suitable. Based on the existing data, we can predict that these schemes are valid for turbulent flows as long as the Navier linear slip model is available. Our further work is to extend the slip boundary conditions to turbulent flows.

Acknowledgments

We acknowledge the financial support from the National Natural Science Foundation of China (Grant No. 51475179 and No. 51679099), and the Fundamental Research Funds for the Central Universities, HUST. 2016JCTD207.

References

[1] Ebaid A, Mutairi F, Khaled S. Effect of velocity slip boundary condition on the flow and heat transfer of cu-water and tio2-water nanofluids in the presence of a magnetic field. Adv Math Phys 2014;2014:538950. doi:10.1155/2014/538950.
[2] Ligrani P, Blanchard D, Gale B. Slip due to surface roughness for a newtonian liquid in a viscous microscale disk pump. Phys Fluids 2010;22(5):052002. doi:10.1063/1.3419081.
[3] Li Y, Bhushan B. The effect of surface charge on the boundary slip of various oleophilic/phobic surfaces immersed in liquids. Soft Matter 2015;11(38):7680–95. doi:10.1039/c5sm00763a.
[4] Hayat T, Farooq S, Alsaedi A, Ahmad B. Influence of variable viscosity and radial magnetic field on peristalsis of copper-water nanomaterial in a non-uniform porous medium. Int J Heat Mass Transf 2016;103:1133–43. doi:10.1016/j.ijheatmasstransfer.2016.07.101.
[5] Lessel M, McGraw JD, Baumchen O, Jacobs K. Nucleated dewetting in supported ultra-thin liquid films with hydrodynamic slip. Soft Matter 2017;13:4756–60. doi:10.1039/C7SM00869D.
[6] Tao S, Zhang H, Guo Z. Drag correlation for micro spherical particles at finite Reynolds and Knudsen numbers by lattice Boltzmann simulations. J Aerosol Sci 2017;103:105–16. doi:10.1016/j.jaerosci.2016.10.006.
[7] Gupta R, Alam M. Hydrodynamics, wall-slip, and normal-stress differences in rarefied granular poiseuille flow. Phys Rev E 2017;95:022903. doi:10.1103/PhysRevE.95.022903.
[8] Ramisetti SB, Borg MK, Lockerby DA, Reese JM. Liquid slip over gas nanofilms. Phys Rev Fluids 2017;2:084003. doi:10.1103/PhysRevFluids.2.084003.
[9] Duan Z. Second-order gaseous slip flow models in long circular and noncircular microchannels and nanochannels. Microfluid Nanofluid 2012;12(5):805–20. doi:10.1007/s10404-011-0924-0.
[10] Karimipour A. New correlation for nusselt number of nanofluid with ag / al2o3 / cu nanoparticles in a microchannel considering slip velocity and temperature jump by using lattice Boltzmann method. Int J Therm Sci 2015;91:146–56. doi:10.1016/j.ijthermalsci.2015.01.015.
[11] Nikkhah Z, Karimipour A, Safaei MR, Forghani-Tehrani P, Goodarzi M, Dahari M, et al. Forced convective heat transfer of water/functionalized multi-walled carbon nanotube nanofluids in a microchannel with oscillating heat flux and slip boundary condition. Int Commun Heat Mass Transfer 2015;68:69–77. doi:10.1016/j.icheatmasstransfer.2015.08.008.
[12] Karimipour A, Nezhad AH, Dí Orazio A, Esfe MH, Safaei MR, Shirani E. Simulation of copper¿cwater nanofluid in a microchannel in slip flow regime using the lattice Boltzmann method. Eur J Mech B/Fluids 2015;49:89–99. doi:10.1016/j.euromechflu.2014.08.004.
[13] Bakli C, Chakraborty S. Slippery to sticky transition of hydrophobic nanochannels. Nano Lett 2015;15:7497–9502. doi:10.1021/acs.nanolett.5b03082.
[14] Wu Y, Xue Y, Pei X, Cai M, Duan H, Huck W, et al. Adhesion-regulated switchable fluid slippage on superhydrophobic surfaces. J Phys Chem 2014;118:2564–9. doi:10.1021/jp411083g.
[15] Sega M, Sbragaglia M, Biferale L, Succi S. The importance of chemical potential in the determination of water slip in nanochannels. Eur Phys J E 2015;38(127):15127. doi:10.1140/epje/i2015-15127-y.
[16] Priezjev N. Molecular diffusion and slip boundary conditions at smooth surfaces with periodic and random nanoscale textures. J Chem Phys 2011;135(20):20470. doi:10.1063/1.3663384.
[17] Nie X, Doolen G, Chen S. Lattice-Boltzmann simulations of fluid flows in mems. J Stat Phys 2002;107:279–89. doi:10.1023/A:1014523007427.
[18] Verhaeghe F, Luo L, Blanpain B. Lattice Boltzmann modeling of microchannel flow in slip flow regime. J Comput Phys 2009;288(4):147–57. doi:10.1016/j.jcp.2008.09.004.
[19] Cui S, Hong N, Shi B, Chai Z. Discrete effect on the halfway bounce-back boundary condition of multiple-relaxation-time lattice Boltzmann model for convection-diffusion equations. Phys Rev E 2016;93:043311. doi:10.1103/PhysRevE.93.043311.
[20] Jahanshaloo L, Sidik NAC, Fazeli A, Mahmoud Pesaran HA. An overview of boundary implementation in lattice Boltzmann method for computational heat and mass transfer. Int Commun Heat Mass Transfer 2016;78:1–12. doi:10.1016/j.icheatmasstransfer.2016.08.014.
[21] Lim C, Shu C, Niu X, Chew Y. Application of lattice Boltzmann method to simulate microchannel flows. Phys Fluids 2002;14(7):2299–308. doi:10.1063/1.1483841.
[22] Ansumali S, Karlin IV. Kinetic boundary conditions in the lattice Boltzmann method. Phys Rev E 2002;66:026311. doi:10.1103/PhysRevE.66.026311.
[23] Succi S. Mesoscopic modeling of slip motion at fluid-solid interfaces with heterogeneous catalysis. Phys Rev Lett 2002;89(6):064502. doi:10.1103/PhysRevLett.89.064502.
[24] Sbragaglia M, Succi S. Analytical calculation of slip flow in lattice Boltzmann models with kinetic boundary conditions. Phys Fluids 2005;17(9):093602. doi:10.1063/1.2044829.
[25] Guo Z, Shi B, Zhao T, Zheng C. Discrete effects on boundary conditions for the lattice Boltzmann equation in simulating microscale gas flows. Phys Rev E 2007;76:056704. doi:10.1103/PhysRevE.76.056704.
[26] Szalmás L. Slip-flow boundary condition for straight walls in the lattice Boltzmann model. Phy Rev E 2006;73:066710. doi:10.1103/PhysRevE.73.066710.
[27] Chai Z, Shi B, Guo Z, Lu J. Gas flow through square arrays of circular cylinders with Klinkenberg effect: A lattice Boltzmann study. Commun Comput Phys 2010;8:1052–73. doi:10.4208/cicp.010809.081209a.
[28] Guo Z, Shi B, Zheng C. Velocity inversion of micro cylindrical couette flow: a lattice Boltzmann study. Comput Math Appl 2011;61(12):3519–27. doi:10.1016/j.camwa.2010.01.022.
[29] Silva G, Semiao V. Consistent lattice Boltzmann modeling of low-speed isothermal flows at finite Knudsen numbers in slip-flow regime: application to plane boundaries. Phys Rev E 2017;96:013311. doi:10.1103/PhysRevE.96.013311.
[30] Singh S, Jiang F, Tsuji T. Impact of the kinetic boundary condition on porous media flow in the lattice Boltzmann formulation. Phys Rev E 2017;96:013303. doi:10.1103/PhysRevE.96.013303.
[31] Asmolov ES, Schmieschek S, Harting J, Vinogradova OI. Flow past superhydrophobic surfaces with cosine variation in local slip length. Phys Rev E 2013;87:023005. doi:10.1103/PhysRevE.87.023005.
[32] Wang L, Yin X. Apparent permeability of flow through periodic arrays of spheres with first-order slip. Powder Technol 2017;311:313–27. doi:10.1016/j.powtec.2017.01.072.
[33] Ahmed N, Hecht M. A boundary condition with adjustable slip length for lattice Boltzmann simulations. J Stat Mech 2009;2009(9):P09017. doi:10.1088/1742-5468/2009/09/P09017.
[34] Reis T, Dellar P. Lattice Boltzmann simulations of pressure-driven flows in microchannels using Navier–Maxwell slip boundary conditions. Phys Fluids 2012;24(11):11200. doi:10.1063/1.4764514.
[35] Švec O, Skoçek J. Simple Naviers slip boundary condition for the non-newtonian lattice Boltzmann fluid dynamics solver. J Non-Newton Fluid Mech 2013;199:61–9. doi:10.1016/j.jnnfm.2013.06.003.
[36] Hyväluoma J, Kunert C, Harting J. Simulations of slip flow on nanobubble-laden surfaces. J Phys 2011;23:184106. doi:10.1088/0953-8984/23/18/184106.
[37] Wang K, Zhang Y, Yu Y, Hou G, Zhou F, Wu Y. Simulation of boundary slip on a liquid-solid surface based on the lattice Boltzmann method. ScienceAsia 2015;41(2):130–5. doi:10.2306/scienceasia1513-1874.2015.41.130.
[38] Guo Z, Zheng C, Shi B. Discrete lattice effects on the forcing term in the lattice Boltzmann method. Phys Rev E 2002;65(4):046308. doi:10.1103/PhysRevE.65.046308.

[39] Choi C, Kim C. Large slip of aqueous liquid flow over a nanoengineered superhydrophobic surface. Phys Rev Lett 2006;96:066001. doi:10.1103/PhysRevLett.96.066001.
[40] Joly L, Biben T. Wetting and friction on superoleophobic surfaces. Soft Matter 2009;5:2549–57. doi:10.1039/b821214g.
[41] Joseph P, Tabeling P. Direct measurement of the apparent slip length. Phys Fluids 2005;71:035303(R). doi:10.1103/PhysRevE.71.03530.
[42] Hooman K, Ejlali A. Effects of viscous heating, fluid property variation, velocity slip, and temperature jump on convection through parallel plate and circular microchannels. Int Commun Heat Mass 2010;37(1):34–8. doi:10.1016/j.icheatmasstransfer.2009.09.011.
[43] Zhang YH, Qin RS, Sun YH, Barber RW, Emerson DR. Gas flow in microchannels –a lattice Boltzmann method approach. J Stat Phys 2005;121:257–67. doi:10.1007/s10955-005-8416-9.
[44] Brinkman HC. The viscosity of concentrated suspensions and solutions. J Chem Phys 1952;20:571–81. doi:10.1063/1.1700493.
[45] He X., Luo L. Lattice Boltzmann model for the incompressible Navier–Stokes equation. J Stat Phys 88(3):927–944. doi: 10.1023/B:JOSS.0000015179.12689.e4
[46] San O., Staples A.E. Dynamics of pulsatile flows through elastic microtubes. Int J Appl Mech 2012;4(1):1250006. doi: 10.1142/S175882511200135X.